

Article

Application of a Response Surface Method for the Optimization of the Hydrothermal Synthesis of Magnetic NiCo₂O₄ Desulfurization Catalytic Powders

Yinke Zhang ¹, Lu Li ¹, Zihan Shang ² and Hang Xu ^{2,*}¹ School of Mathematics and Statistics, Henan University of Science and Technology, Luoyang 471023, China² School of Chemistry and Chemical Engineering, Henan University of Science and Technology, Luoyang 471023, China

* Correspondence: xhinbj@126.com

Abstract: In this study, nickel cobaltate (NiCo₂O₄) powders are employed as a catalyst in conjunction with persulfate for the development of a catalytic oxidation system to enhance fuel desulfurization. The hydrothermal synthesis conditions of NiCo₂O₄ powders, which significantly influenced the desulfurization efficiency, were optimized using a response surface methodology with a Box–Behnken design. These conditions were ranked in the following order: calcination temperature > hydrothermal temperature > calcination time > hydrothermal time. Through the optimization process, the ideal preparation conditions were determined as follows: a hydrothermal temperature of 143 °C, hydrothermal time of 6.1 h, calcination temperature of 330 °C, and calcination time of 3.7 h. Under these optimized conditions, the predicted desulfurization rate was approximately 85.8%. The experimental results closely matched the prediction, yielding a desulfurization rate of around 84%, with a minimal error of only 2.1%. To characterize the NiCo₂O₄ powders prepared under the optimal conditions, XRD, SEM, and TEM analyses were conducted. The analysis revealed that the microscopic morphology of NiCo₂O₄ exhibited a rectangular sheet structure, with an average particle size of 20 nm. Additionally, fan-shaped NiCo₂O₄ particles were observed as a result of linear and bundle agglomerations. Thus, this work is innovative in its ability to synthesize nano-catalysts using hydrothermal synthesis in a controllable manner and establishing a correlation between the hydrothermal synthesis conditions and catalytic activity.

Keywords: response surface methodology; hydrothermal synthesis; nickel cobaltate; desulfurization; optimization



Citation: Zhang, Y.; Li, L.; Shang, Z.; Xu, H. Application of a Response Surface Method for the Optimization of the Hydrothermal Synthesis of Magnetic NiCo₂O₄ Desulfurization Catalytic Powders. *Catalysts* **2023**, *13*, 1119. <https://doi.org/10.3390/catal13071119>

Academic Editor: Haralampos N. Miras

Received: 24 June 2023

Revised: 12 July 2023

Accepted: 15 July 2023

Published: 18 July 2023



Copyright: © 2023 by the authors. Licensee MDPI, Basel, Switzerland. This article is an open access article distributed under the terms and conditions of the Creative Commons Attribution (CC BY) license (<https://creativecommons.org/licenses/by/4.0/>).

1. Introduction

Hydrothermal synthesis is widely utilized in the preparation of nano-powders due to its distinct advantages. It offers high particle dispersion, uniform and easily controllable particle size distribution, as well as good particle purity. This method operates under subcritical conditions with temperatures ranging from 100–240 °C and pressures from 0.3–4 MPa [1]. In 1996, Qian successfully synthesized GaN nanocrystals using benzene thermal synthesis, which marked a significant milestone in the field of the hydrothermal (solvent heat) synthesis of nanomaterials [2]. Since then, the hydrothermal synthetic method has gained popularity in various fields, including crystalline materials [3], ceramic materials, molecular sieve materials [4], nanomaterials, electrode materials [5], catalytic materials, and more.

Nickel cobaltate (NiCo₂O₄) exhibits an excellent performance as a material in supercapacitors [6], direct catalytic oxidation [7], photocatalysis [8], electrocatalysis [9], and other applications. Particularly, it is often employed as a catalyst coupled with oxidants, such as hydrogen peroxide, ozone, or persulfate, forming Fenton-like oxidation systems for the degradation of organic pollutants [10]. Zhou et al. utilized a co-precipitation hydrothermal

method to synthesize NiCo_2O_4 , which acted as a catalyst for peroxymonosulfate (PMS) in the degradation of citric acid in water [11]. It is indeed challenging to achieve the precise control of particle morphology using the co-precipitation method. The sol-gel method is a commonly used approach for synthesizing nanostructured NiCo_2O_4 materials. However, this method also faces challenges in controlling the morphology and size of the resulting particles. Additionally, the sol-gel method often leads to significant product non-uniformity, which hinders large-scale industrial production [12]. Similarly, Xu et al. employed a simple hydrothermal method to load NiCo_2O_4 onto expanded graphite, creating a catalyst that was coupled with PMS to decompose sulfamethoxazole, focusing on the oxidizing agent properties of the species involved [13]. Tian et al. also used a straightforward hydrothermal method to synthesize dandelion-shaped NiCo_2O_4 microspheres, which were coupled with PMS to form a Fenton-like system for the degradation of humic acids in water, exhibiting an excellent performance [14]. In a previous study, we successfully synthesized sea urchin-shaped NiCo_2O_4 using a simple hydrothermal method, and coupled it with PMS to catalyze the oxidative removal of dibenzothiophene (DBT) from octane, demonstrating excellent activity [15]. The NiCo_2O_4 as a catalyst can also be applied in various aspects, such as methanol conversion and combustion [16,17], propane oxidation [18], electrode materials [19], and so on.

Based on the literature analysis, it is evident that previous studies focused primarily on determining specific conditions for hydrothermal synthesis to achieve desired microstructures of NiCo_2O_4 . The hydrothermal synthesis of NiCo_2O_4 in an aqueous solution offers the advantage of efficient mixing and heat transfer, leading to the uniform dispersion of reactants and precise control over the reaction process. This results in the generation of high-quality materials with consistent properties. Moreover, this approach enables the manipulation of product morphology, size, and structure, thereby influencing the catalytic activity of NiCo_2O_4 . The hydrothermal synthesis method can also be utilized for synthesizing various oxides, such as ZnMoO_4 [20], NiMoO_4 [21], Sn_3O_4 [22], and SAPO-18 [23], and can be applied in specific catalytic processes.

To address the scarcity of studies focusing on optimizing hydrothermal synthesis conditions, this study employs a response surface methodology (RSM). RSM is a statistical method widely utilized in experimental optimization processes across various fields, including chemistry, food, environment, and materials [24]. In the context of desulfurization, dibenzothiophene (DBT) is used as a representative sulfur-containing compound, octane is used as a simulated oil, peroxymonosulfate (PMS) serves as the oxidant, and acetonitrile acts as the extractant. The four hydrothermal synthesis conditions, hydrothermal temperature, hydrothermal time, calcination temperature, and calcination time are optimized using RSM to determine the optimal preparation conditions for achieving the highest desulfurization activity with the NiCo_2O_4 catalyst. The goal of this study is to establish the relationship between the powder preparation conditions and the resulting catalytic activity.

2. Results and Discussion

2.1. Desulfurization Experimental Results and Modeling

Table 1 shows 29 sets of experiments arranged by the Box–Behnken design principle on Design Expert 8.0.6. The desulfurization experiments were performed according to the experimental conditions arranged by the design to obtain the corresponding desulfurization rates. A second-order model of the desulfurization rate (Y) versus the four conditions of hydrothermal temperature (A), hydrothermal time (B), calcination temperature (C), and calcination time (D) for the preparation of NiCo_2O_4 powders was established as shown in Equation (1):

$$Y = 83.80 + 1.78A + 0.80B - 4.68C - 1.59D + 0.075AB + 0.52AC + 1.05AD + 1.3BC - 2.52BD - 0.5CD - 4.50A^2 - 6.85B^2 - 5.54C^2 - 5.09D^2 \quad (1)$$

Table 1. Box–Behnken experimental arrangement and desulfurization rates [25,26].

Runs	Hydrothermal Temperature (A)/°C	Hydrothermal Time (B)/h	Calcination Temperature (C)/°C	Calcination Time (D)/h	Desulfurization Rate (Y)/%
1	160	6	400	4	71.6
2	140	6	350	4	85.1
3	160	6	300	4	80.7
4	140	3	300	4	75.2
5	140	9	400	4	68.7
6	120	6	350	6	68.3
7	140	9	350	6	67.2
8	140	6	300	2	78.3
9	160	6	350	2	76.5
10	120	9	350	4	73.2
11	160	3	350	4	72.6
12	160	6	350	6	73.3
13	140	6	350	4	82.5
14	140	6	300	6	77.8
15	120	3	350	4	69.7
16	160	9	350	4	76.4
17	120	6	400	4	66.2
18	140	9	300	4	75.3
19	140	6	400	6	68.1
20	140	3	400	4	63.4
21	140	6	350	4	85.8
22	120	6	300	4	77.4
23	120	6	350	2	75.3
24	140	6	350	4	81.9
25	140	6	350	4	83.7
26	140	3	350	2	71.9
27	140	9	350	2	75.4
28	140	3	350	6	73.8
29	140	6	400	2	70.6

Figure 1 shows a comparison between the predicted desulfurization values (regression values) calculated using the second-order model, Equation (1), and the corresponding experimental values. The plot demonstrates that the regression and experimental values are primarily distributed along the diagonal of the coordinate system. There is a lack of data points that significantly deviate from the diagonal line, indicating that the residuals of the model are small and the model itself is reasonable. This observation suggests that the second-order model adequately represents the relationship between the desulfurization rate and the four experimental conditions for the preparation of NiCo₂O₄ powders. The close alignment of the regression values with the experimental values supports the accuracy and validity of the model in predicting the desulfurization rates based on the chosen hydrothermal synthesis conditions.

Figure 2 displays the internally studentized residuals corresponding to the 29 experimental runs. The plot reveals that the residuals exhibited irregular characteristics, indicating that the experimental errors stemmed from random fluctuations rather than systematic errors. Notably, the range of the internally studentized residuals remained within -2 to 2 , suggesting that there were no significant outliers or faulty measurements in the experimental results. No residuals exceed -3 and 3 , indicating the correctness of the fitting formula and the absence of significant residuals. This further supports the reliability and validity of the obtained data. The absence of residuals outside the -2 to 2 range indicates that the experimental results are consistent with the predicted values from the second-order model, confirming the overall robustness of the experimental setup and the accuracy of the desulfurization rate measurements.

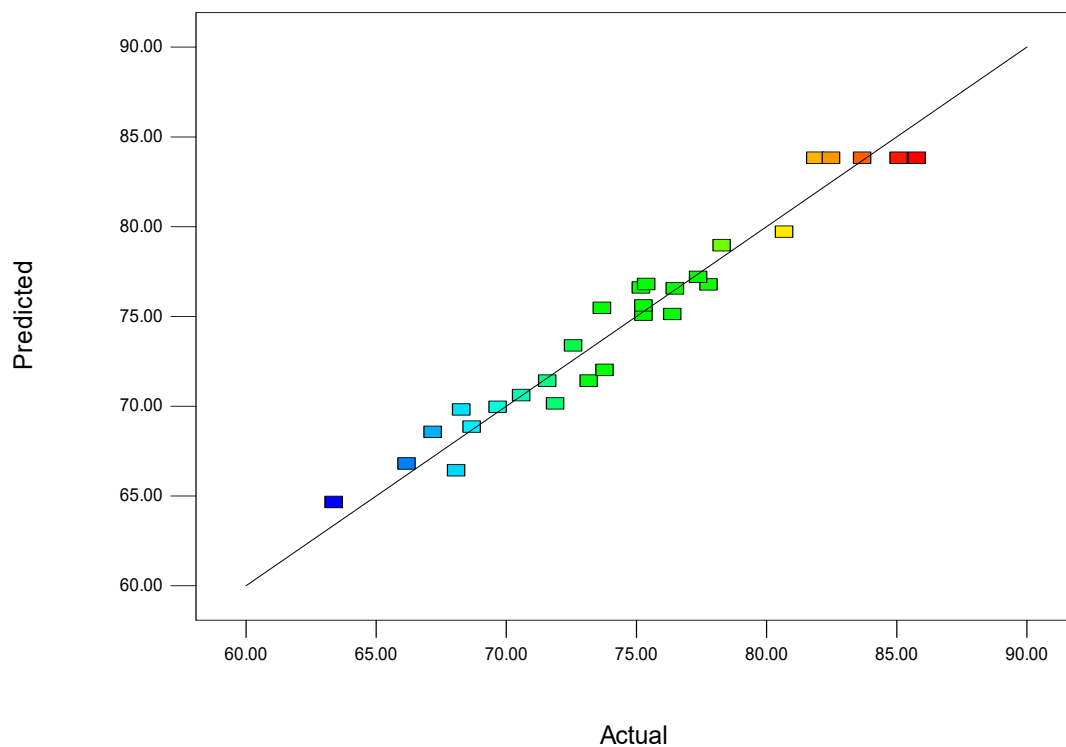


Figure 1. Comparison of predicted and experimental values based on the second-order model.

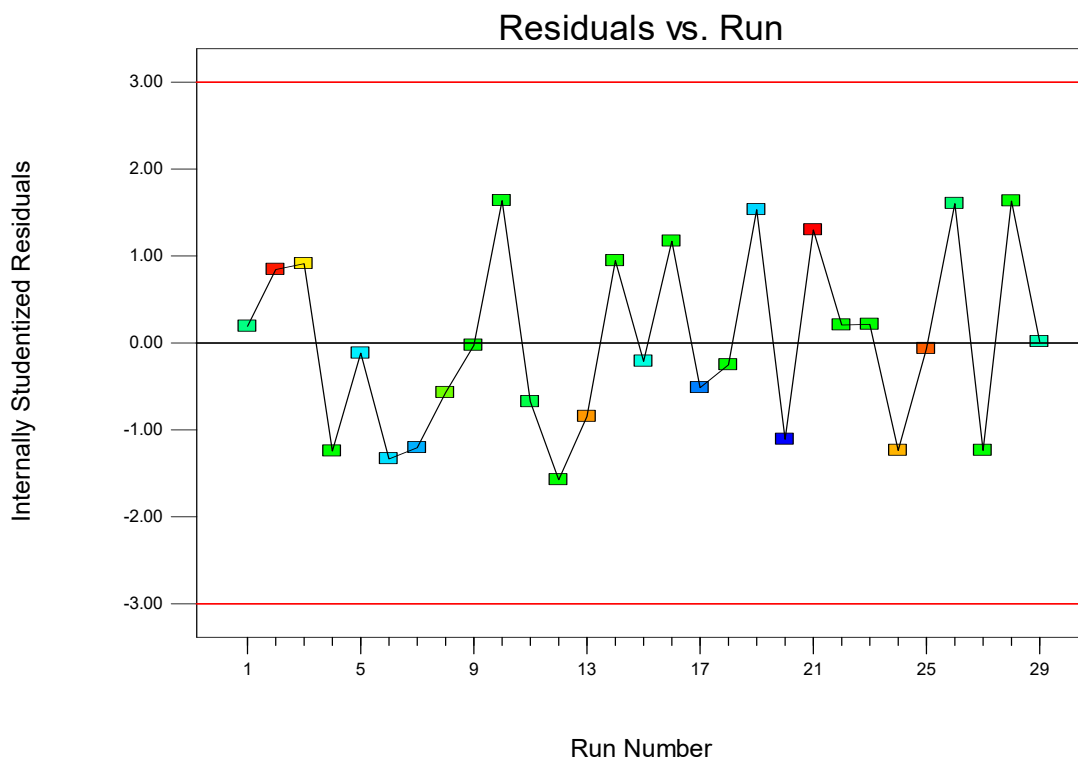


Figure 2. The internally studentized residuals at run number from 1 to 29.

2.2. Analysis of Variance (ANOVA)

Table 2 provides the analysis of variance (ANOVA) for the response surface second-order model. The F-value was 21.8, with a *p*-value (<0.0001) significantly less than 0.01, indicating that the model obtained through the response surface method was highly signifi-

cant. Analyzing Table 2 reveals that the desulfurization rate (Y) is primarily influenced by hydrothermal temperature (A), calcination temperature (C), and calcination time (D), as evidenced by their low p -values (<0.05). In contrast, hydrothermal time (B) had a relatively lower impact, as its p -value exceeded 0.05. This observation was further supported by the coefficient values in Equation (1), where the coefficients associated with hydrothermal temperature (A), calcination temperature (C), and calcination time (D) were significantly greater than the coefficient for hydrothermal time (B). The interaction between hydrothermal time (B) and calcination time (D), represented by the BD term, was found to be significant (p -value = 0.0108), while other interactions, such as AB, AC, AD, BC, and CD, could be considered negligible. This suggested that the interaction between the four conditions was not substantial. Based on the mean square data and F-values, it was observed that calcination temperature (C) had the highest impact on the desulfurization rate, followed by hydrothermal temperature (A), calcination time (D), and hydrothermal time (B). Additionally, the squared terms A^2 , B^2 , C^2 , and D^2 were all extremely significant, indicating a non-linear relationship between the desulfurization rate (Y) and the respective factors A, B, C, and D. The residual term's sum of squares and mean square values were relatively low at 41.37 and 2.96, respectively, indicating that the fitted desulfurization rate was not significantly different from the experimental desulfurization rate. The misfit term's F-value was 1.104 with a p -value of 0.5034, suggesting no significant correlation between the model misfit and the pure difference, indicating a good fit for the model. The mean value of the desulfurization rate was reported as 74.7. The precision of the model measurement was 15.5 (>4), and the coefficient of variation was 2.3% ($<4\%$), both indicating the high accuracy of the experiments. The fitted correlation coefficient $R^2 = 0.95$ indicated the correctness of the obtained model. The difference between Adj R^2 and Pred R^2 was 0.12, which was less than 0.2, implying the reasonableness of the obtained second-order model. Overall, the ANOVA results established the correctness and significance of the second-order model derived using the response surface method.

Table 2. ANOVA table for the response surface second-order model of the desulfurization rate.

Source	Sum of Squares	df	Mean Square	F-Value	p -Value	Significance
model	901.5708	14	64.39792	21.7933	<0.0001	**
A	38.16333	1	38.16333	12.91509	0.0029	**
B	7.68	1	7.68	2.599037	0.1292	Not Significant
C	262.2675	1	262.2675	88.75559	<0.0001	**
D	30.40083	1	30.40083	10.28814	0.0063	**
AB	0.0225	1	0.0225	0.007614	0.9317	Not Significant
AC	1.1025	1	1.1025	0.373104	0.5511	Not Significant
AD	4.41	1	4.41	1.492416	0.2420	Not Significant
BC	6.76	1	6.76	2.287694	0.1526	Not Significant
BD	25.5025	1	25.5025	8.630461	0.0108	*
CD	1	1	1	0.338416	0.5700	Not Significant
A^2	131.5947	1	131.5947	44.53379	<0.0001	**
B^2	304.7325	1	304.7325	103.1265	<0.0001	**
C^2	199.2005	1	199.2005	67.41268	<0.0001	**
D^2	168.1626	1	168.1626	56.90897	<0.0001	**
Residual	41.36917	14	2.95494			
Lack of fit	30.36917	10	3.036917	1.104333	0.5034	Not Significant
Pure error	11	4	2.75			
Cor total	942.94	28				
Std. Dev.		1.72		R^2	0.9561	
Mean		74.7		Adj R^2	0.9123	
C.V.%		2.3		Pred R^2	0.7963	
PRESS		192.11	Adeq precisor		15.507	

* Significant ($p < 0.05$), ** extremely significant ($p < 0.01$).

2.3. Response Surface Analysis

Figure 3 illustrates the response surface plots depicting the effects of hydrothermal temperature (A), hydrothermal time (B), calcination temperature (C), and calcination time (D) on the desulfurization rate. From the figure, it is evident that these factors exhibit a trend of an increasing and then decreasing impact on the desulfurization rate. This suggests the presence of optimal experimental conditions within the selected range. The color gradient from the edge to the center of the surface signifies a gradual increase in the response value (desulfurization rate). The highest point of the response surface, denoted by the center of the minimum ellipse, represents the optimized preparation conditions achieved through the response surface method.

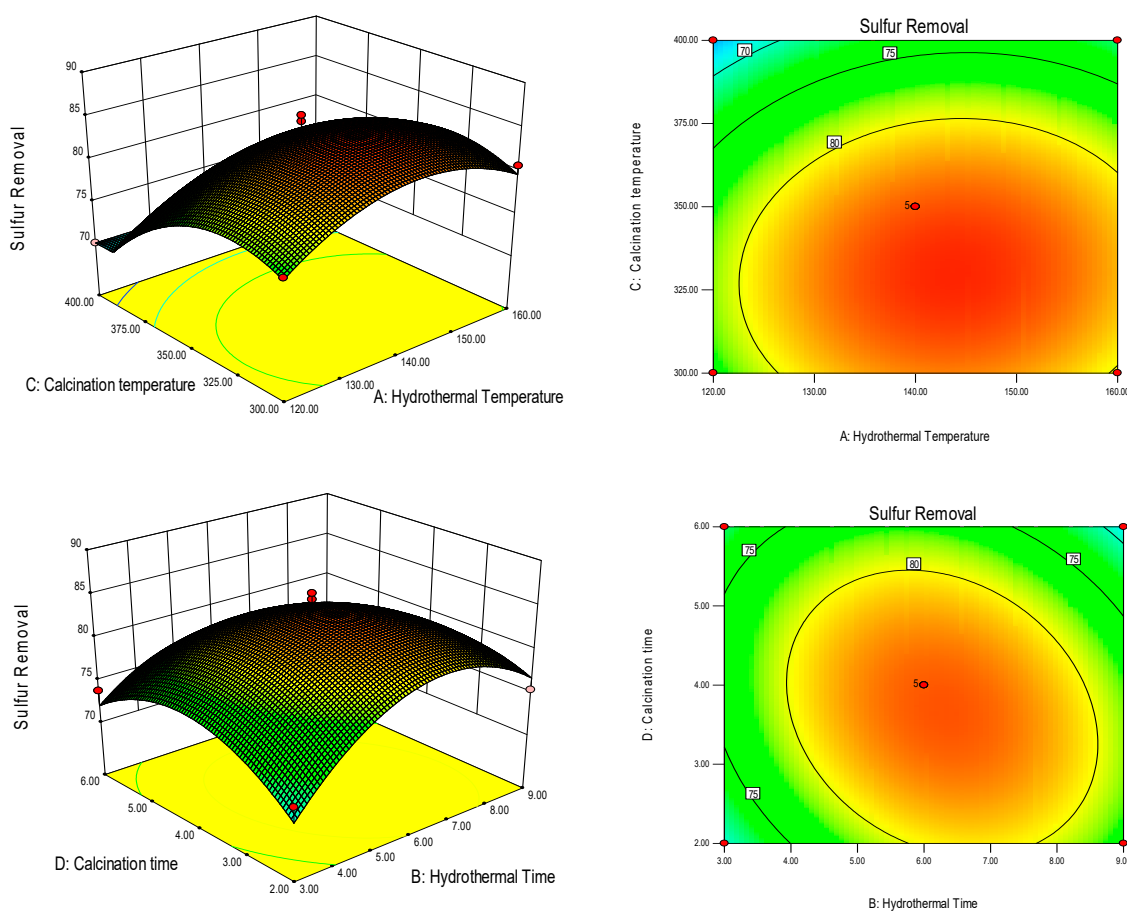


Figure 3. Response surface plot of the effect of hydrothermal temperature (A), hydrothermal time (B), calcination temperature (C), and calcination time (D) on the desulfurization rate.

Analyzing Figure 3 further reveals that the contours formed between the hydrothermal temperature (A) and calcination temperature (C) are elliptical, but with small curvature. On the other hand, the contours between hydrothermal time (B) and calcination time (D) also appear elliptical, but with a larger curvature. This indicates that the interaction between hydrothermal temperature (A) and calcination temperature (C) is not significant, while the interaction between hydrothermal time (B) and calcination time (D) is pronounced. Hydrothermal temperature (A) and calcination temperature (C) can be considered independent of each other, without needing to account for their mutual influence. However, when dealing with the time conditions, attention should be given to the interaction between hydrothermal time (B) and calcination time (D), as it has a noticeable impact. Since the influence of hydrothermal time (B) on the desulfurization rate is relatively low, greater emphasis should be placed on considering the influence of calcination time (D) when determining the optimal preparation time conditions.

The reasons behind these observations can be analyzed as follows: during the hydrothermal synthesis of NiCo_2O_4 powders, they undergo a nucleation–growth–agglomeration process. This formation process occurs rapidly, requiring only a relatively short time to complete the hydrothermal process. Consequently, the influence of hydrothermal time (B) on the desulfurization rate is relatively minor. Hydrothermal temperature (A) exerts a greater impact on particle morphology. Increasing the temperature enhances the molecular movement, facilitating particle nucleation but hindering growth and agglomeration, thereby significantly affecting the desulfurization effectiveness of the powders. Calcination temperature (C) plays a crucial role in removing inorganic and organic substances from the powder surface during the hydrothermal process. It directly affects the formation and transformation process of NiCo_2O_4 crystalline structures, as well as the particle size. Consequently, it has a significant influence on the desulfurization rate. The pronounced effect of calcination time (D) can be attributed to inadequate removal rates of inorganic and organic matter from the powder surface in shorter durations. Additionally, slower NiCo_2O_4 crystalline formation and the time required for temperature conduction to the powder in the muffle furnace contribute to the notable influence of calcination time (D) on the desulfurization process.

2.4. Optimal Experimental Conditions from RSM and NiCo_2O_4 Characterization

Figure 4 presents the optimized NiCo_2O_4 preparation conditions obtained through the response surface method. These conditions included a hydrothermal temperature of 143 °C, hydrothermal time of 6.1 h, calcination temperature of 330 °C, and calcination time of 3.7 h. The predicted desulfurization rate corresponding to these conditions was 85.8%. The synthesis results achieved using the optimized NiCo_2O_4 preparation conditions are displayed in Figure 5. The XRD characterization results of the synthesized NiCo_2O_4 , as shown in Figure 5, precisely match the JCPDS card (20–0781). The characteristic peaks of 2θ are located at 18.90°, 31.15°, 36.70°, 38.40°, 44.62°, 55.43°, 59.09°, 64.98°, and 77.54°, corresponding to the (111), (220), (311), (222), (400), (422), (511), (440), and (533) crystal planes of cubic NiCo_2O_4 . This indicates the successful synthesis of pure NiCo_2O_4 powders. Furthermore, the excellent magnetic separation properties of the material can be observed in Figure 5, where the powders can be separated from acetonitrile using a magnet. This suggests that the material possesses strong magnetic separation capabilities. The SEM image presented in Figure 4 illustrates that the particles of NiCo_2O_4 are at the nano-level and arranged in a linear agglomeration pattern.

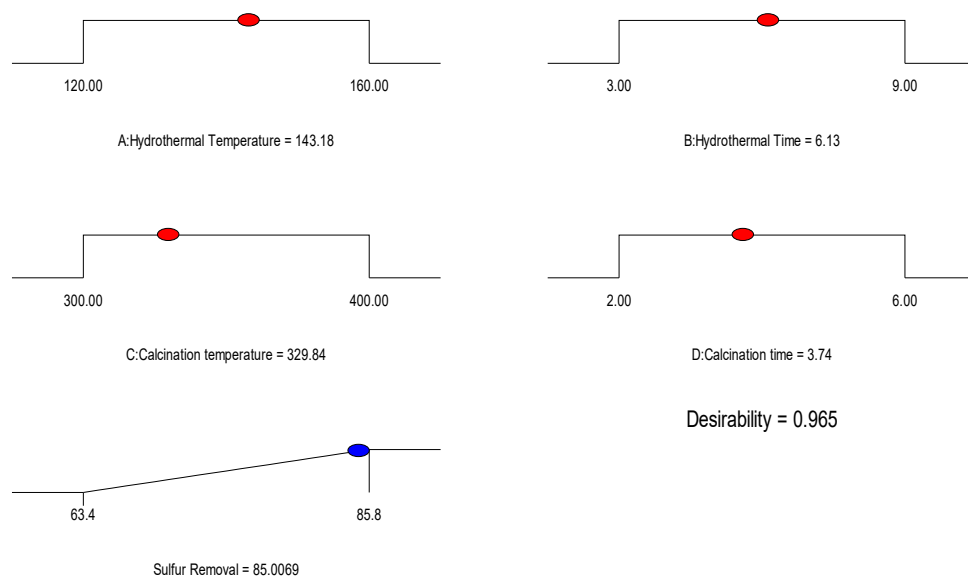


Figure 4. Optimal experimental conditions from RSM.

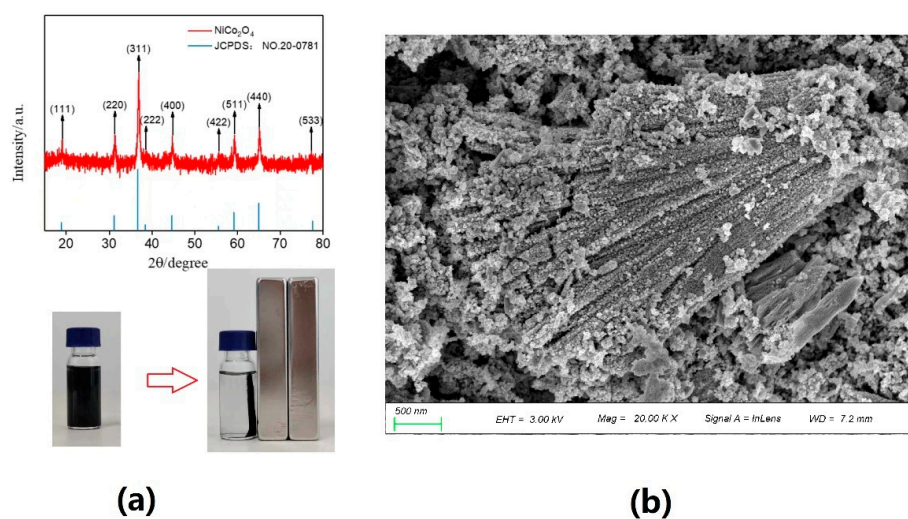


Figure 5. XRD (a) and SEM (b) images of NiCo_2O_4 powders.

Figure 6 displays the TEM analysis of NiCo_2O_4 powders, providing a further insight into the agglomeration mechanism of the particles. The analysis revealed a clear progression in the formation process of NiCo_2O_4 powders. Initially, NiCo_2O_4 nuclei were observed to nucleate, resulting in the formation of rectangular-shaped particles with an average particle size of approximately 20 nm. These nuclei served as the initial building blocks for further agglomeration. Subsequently, the nuclei underwent primary linear agglomeration, leading to the formation of nanowires. This primary agglomeration process involved the alignment and connection of the individual rectangular-shaped particles, resulting in the elongated structure of the nanowires. Following primary agglomeration, the nanowires underwent a secondary bundled agglomeration. This process involved the bundling or clustering of multiple nanowires together, leading to the formation of larger structures. Finally, the agglomeration process culminated in the formation of fan-shaped NiCo_2O_4 powders. These powders exhibited a distinctive fan-like morphology, which was the result of the secondary bundled agglomeration of the nanowires. Overall, the TEM analysis provided a comprehensive view of the agglomeration mechanism of NiCo_2O_4 powders, illustrating the sequential progression from nuclei formation to primary linear agglomeration, followed by secondary bundled agglomeration, and ultimately resulting in the formation of fan-shaped powders.

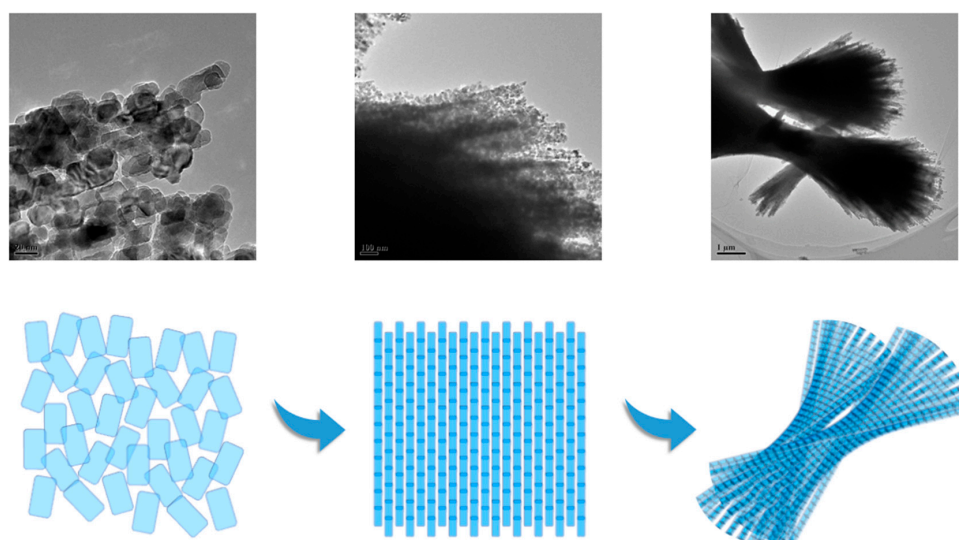


Figure 6. TEM of NiCo_2O_4 and the formation mechanism of the powders.

2.5. Desulfurization Cycle Experiment of NiCo_2O_4 Powders

Figure 7 presents the experimental results of the desulfurization cycle using the prepared NiCo_2O_4 powders. The figure demonstrates that the desulfurization rate achieved with the NiCo_2O_4 powders is approximately 84%. Additionally, it can be observed that the activity of the powder remains consistent, even after six cycles, indicating its excellent recycling performance. Comparing the experimental desulfurization rate of 84% with the predicted value of 85.8% (red dash line), it can be deduced that the error between the predicted and actual values is only around 2.1%. This suggests that the predicted desulfurization rate obtained through the response surface method is highly accurate. The close agreement between the predicted and experimental results further validates the effectiveness and reliability of the response surface model in optimizing the preparation conditions for NiCo_2O_4 powders. The minimal error indicates the success of the optimization process and reinforces the suitability of the obtained conditions for achieving high desulfurization rates.

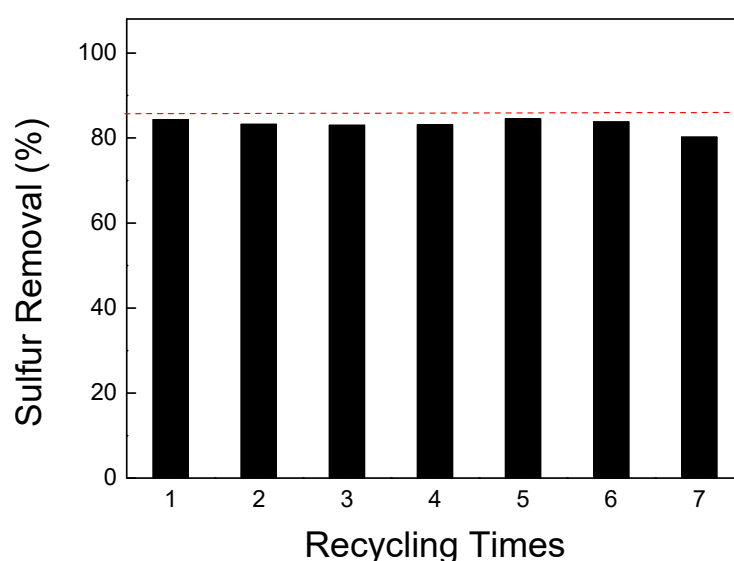


Figure 7. Cyclic desulfurization experiment of NiCo_2O_4 powders.

3. Experimental

3.1. Preparation of NiCo_2O_4 Powders by Hydrothermal Synthesis

Dissolve 1.1897 g of CoCl_2 , 0.5942 g of NiCl_2 , 0.9109 g of cetyltrimethyl ammonium bromide, and 1.35 g of urea in 37.5 mL of deionized water. Stir the mixture magnetically for 20 min. Transfer the solution to a hydrothermal kettle with a PTFE liner. Subject the solution to different hydrothermal times and temperatures. Collect the resulting powders by magnetic separation. Purify the collected powders by washing with ethanol. Dry the purified material under vacuum at 70 °C for 4 h. Calcine the dried material at different times and temperatures to obtain NiCo_2O_4 powder. It is worth mentioning that the reagents used for the experiments were purchased from Shanghai Aladdin Reagent Company (Shanghai, China).

3.2. Designing Experiments by Response Surface Method

The experimental ranges for the four hydrothermal synthesis conditions were determined based on pre-experiments in the previous section. These ranges were as follows: hydrothermal temperature (A) of 120–160 °C, hydrothermal time (B) of 3–9 h, calcination temperature (C) of 300–400 °C, and calcination time (D) of 2–6 h. To design the experiments, a Box–Behnken design (BBD) was implemented using Design-Expert 8.0.6 software. The BBD design involved setting up four experimental levels and codes, which are shown in Table 3. For each factor, three levels were designed, including a cubic point with coded

values of 1 and -1 , and a central point with a coded value of 0. Additionally, five replicate experiments were conducted at the center point (coded 0) to test repeatability, rationality, random error, and reduce systematic errors. In total, 29 desulfurization experiments were performed using the response surface method based on the experimental levels arranged by the Box–Behnken design. This approach aimed to establish the nonlinear relationship between the experimental results (desulfurization rates) and the four experimental conditions. The accuracy of this relationship was tested using analysis of variance (ANOVA).

Table 3. Level setting table of experimental factors for response surface method.

Factors	Levels			Units
	-1	0	1	
Hydrothermal temperature (A)	120	140	160	$^{\circ}\text{C}$
Hydrothermal time (B)	3	6	9	h
Calcination temperature (C)	300	350	400	$^{\circ}\text{C}$
Calcination time (D)	2	4	6	h

3.3. Characterization of NiCo_2O_4 Powders

The characterization of the NiCo_2O_4 powders was conducted using three different instruments: X-ray diffractometer (XRD): XRD is used to study the crystal structure of materials by analyzing the diffraction pattern produced when X-rays interact with the sample. This technique provides information about the crystalline phases present in the NiCo_2O_4 powders. When performing tests using the PANalytical X'Pert Powder X-ray diffractometer (Almelo, Netherlands), we utilized the following conditions: $\text{CuK}\alpha$ /Graphite monochromator as the X-ray source, with a tube voltage of 40 KV and a tube current of 40 mA. The step angle was set to 0.1° , and a scan rate of $5^{\circ}/\text{min}$ was employed within the range of 10° to 80° . Scanning electron microscope (SEM): the SEM analysis was conducted using a Hitachi Regulus 8100 instrument from Japan (Tokyo). SEM allows for the high-resolution imaging of the surface morphology and topography of materials. It provides detailed information about the particle size, shape, and distribution of the NiCo_2O_4 powders. Transmission electron microscope (TEM): TEM analysis was conducted using a Thermo Fisher FEI Tecnai G2 F20 instrument from the USA (Hillsboro, OH). TEM enables the observation of materials at a very high resolution, allowing for the examination of their atomic-level structure. It provides valuable information about the internal structure, lattice defects, and individual particle characteristics of the NiCo_2O_4 powders. These characterization techniques were employed to gain insights into the structural and morphological properties of the synthesized NiCo_2O_4 powders.

3.4. Desulfurization Experiment

To perform the catalytic oxidative desulfurization, the following procedure was followed: diphenylthiophene (DBT) was dissolved in n-octane to create a simulated oil with an initial sulfur content of 600 ppm. A total of 0.5 g of NiCo_2O_4 powders was added to 6 mL of simulated oil. To this mixture, 2 mL of acetonitrile was added. The mixture was vigorously stirred for 30 min to allow for the equilibrium of adsorption and extraction to be reached. The catalytic oxidative desulfurization was initiated by adding 0.5 mL of PMS (20 wt. %) to the mixture. The reaction was performed at 40°C for a duration of 60 min. After this reaction time, the desulfurization process was considered complete. The supernatants from the reaction were then measured for sulfur content in n-octane using a UV-Vis spectrophotometer (Shimadzu UV-2700, Kyoto, Japan). By measuring the sulfur content in the supernatants, the extent of desulfurization achieved by the catalytic process could be determined.

4. Conclusions

In this study, response surface methodology was utilized to optimize the hydrothermal preparation process of NiCo₂O₄ powders. The desulfurization activity of the synthesized powders was also investigated. Among the factors considered, hydrothermal temperature (A), calcination temperature (C), and calcination time (D) had a significant impact on the desulfurization rate. However, hydrothermal time (B) did not exhibit a substantial effect. The order of significance for the factors was determined as follows: calcination temperature (C) > hydrothermal temperature (A) > calcination time (D) > hydrothermal time (B). Based on the response surface method, the optimal preparation conditions were determined as follows: hydrothermal temperature of 143 °C, hydrothermal time of 6.1 h, calcination temperature of 330 °C, and calcination time of 3.7 h. The predicted desulfurization rate for the NiCo₂O₄ powders prepared under these conditions was 85.8%. In the experimental evaluation, the desulfurization rate achieved was approximately 84%, with an error of only 2.1% compared to the predicted value. The NiCo₂O₄ powders obtained exhibited a rectangular particle shape with an average size of 20 nm. During the agglomeration process, the particles underwent linear and bundled agglomerations, resulting in the formation of fan-shaped NiCo₂O₄ powders. Furthermore, the desulfurization rate of the NiCo₂O₄ powders remained stable throughout six cycles of catalytic oxidation and magnetic separation experiments. This demonstrated the excellent recycling performance of the prepared powders. Overall, the utilization of response surface methodology allowed for the optimization of the hydrothermal preparation process of NiCo₂O₄ powders, leading to high desulfurization rates. The synthesized powders exhibited desirable morphological characteristics and demonstrated an effective desulfurization performance over multiple cycles of operation.

Author Contributions: Experiment, analysis, calculation, writing, Y.Z.; calculation, writing, L.L.; picture, Z.S.; conceptualization, writing and editing, reagents, equipment and supervision, H.X. All authors have read and agreed to the published version of the manuscript.

Funding: This study was supported by the Nature Science Foundation of Henan Province (No: 202300410155).

Data Availability Statement: The data that support the findings of this study are available from the corresponding author, Hang Xu, upon reasonable request.

Conflicts of Interest: The authors declare no conflict of interest.

References

1. Shi, W.; Song, S.; Zhang, H. Hydrothermal synthetic strategies of inorganic semiconducting nanostructures. *Chem. Soc. Rev.* **2013**, *42*, 5714–5743. [[CrossRef](#)] [[PubMed](#)]
2. Xie, Y.; Qian, Y.T.; Wang, W.Z.; Xie, Y.; Qian, Y.; Wang, W.; Zhang, S.; Zhang, Y. A benzene-thermal synthetic route to nanocrystalline GaN. *Science* **1996**, *272*, 1926–1927. [[CrossRef](#)] [[PubMed](#)]
3. Wang, X.; Li, Y. Selected-control hydrothermal synthesis of alpha- and beta MnO₂ single crystal nanowires. *J. Am. Chem. Soc.* **2002**, *124*, 2880–2881. [[CrossRef](#)] [[PubMed](#)]
4. Costa, J.A.S.; Vedovello, P.; Paranhos, C.M. Use of Ionic Liquid as Template for Hydrothermal Synthesis of the MCM-41 Mesoporous Material. *Silicon* **2020**, *12*, 289–294. [[CrossRef](#)]
5. Li, Z.; Yang, J.; Guang, T.; Fan, B.; Zhu, K.; Wang, X. Controlled Hydrothermal/Solvothermal Synthesis of High-Performance LiFePO₄ for Li-Ion Batteries. *Small Methods* **2021**, *5*, 2100193. [[CrossRef](#)]
6. Wang, X.; Fang, Y.; Shi, B.; Huang, F.; Rong, F.; Que, R. Three-dimensional NiCo₂O₄@NiCo₂O₄ core-shell nanocones arrays for high-performance supercapacitors. *Chem. Eng. J.* **2018**, *344*, 311–319. [[CrossRef](#)]
7. Liu, X.; Xu, D.; Zhang, D.; Zhang, G.; Zhang, L. Superior performance of 3D Co-Ni bimetallic oxides for catalytic degradation of organic dye: Investigation on the effect of catalyst morphology and catalytic mechanism. *Appl. Catal. B-Environ.* **2016**, *186*, 193–203. [[CrossRef](#)]
8. Cheng, C.; Mao, L.; Shi, J.; Xue, F.; Zong, S.; Zheng, B.; Guo, L. NiCo₂O₄ nanosheets as a novel oxygen-evolution-reaction cocatalyst in situ bonded on the g-C₃N₄ photocatalyst for excellent overall water splitting. *J. Mater. Chem. A* **2021**, *9*, 12299–12306. [[CrossRef](#)]
9. Ge, R.; Ma, M.; Ren, X.; Qu, F.; Liu, Z.; Du, G.; Asiri, A.M.; Chen, L.; Zheng, B.; Sun, X. A NiCo₂O₄@Ni-Co-Ci core-shell nanowire array as an efficient electrocatalyst for water oxidation at near-neutral pH. *Chem. Commun.* **2017**, *53*, 7812–7815. [[CrossRef](#)]

10. Qian, H.; Hou, Q.; Yu, G.; Nie, Y.; Bai, C.; Bai, X.; Ju, M. Enhanced removal of dye from wastewater by Fenton process activated by core-shell NiCo₂O₄@FePc catalyst. *J. Clean. Prod.* **2020**, *273*, 123028. [[CrossRef](#)]
11. Zhou, X.; Li, X.; Xu, C.; Yang, L.; Yang, G.; Guo, L. A persulfate oxidation system for removing acid orange from aqueous solution: Evaluation and degradation mechanism. *J. Environ. Manag.* **2022**, *322*, 116054. [[CrossRef](#)] [[PubMed](#)]
12. Habibi, M.H.; Sabzyan, H.; Bayranvand, M. Sol-gel preparation, structural, thermal and spectroscopic analyses, and opto-electronic and photocatalytic activities of normal spinel nickel cobaltite nano-powder for photo-degradation of Reactive Red RB. *J. Mater. Sci.-Mater. Electron.* **2017**, *28*, 8546–8553. [[CrossRef](#)]
13. Xu, M.; Zhou, H.; Wu, Z.; Li, N.; Xiong, Z.; Yao, G.; Lai, B. Efficient degradation of sulfamethoxazole by NiCo₂O₄ modified expanded graphite activated peroxymonosulfate: Characterization, mechanism and degradation intermediates. *J. Hazard. Mater.* **2020**, *399*, 123103. [[CrossRef](#)]
14. Tian, X.; Tian, C.; Nie, Y.; Dai, C.; Yang, C.; Tian, N.; Zhou, Z.; Li, Y.; Wang, Y. Controlled synthesis of dandelion-like NiCo₂O₄ microspheres and their catalytic performance for peroxymonosulfate activation in humic acid degradation. *Chem. Eng. J.* **2018**, *331*, 144–151. [[CrossRef](#)]
15. Yuan, Q.; Wu, F.; Xu, H.; Wang, X.; Luo, J.; Song, Y.; Guo, Y.; Wei, X. Preparation of magnetic urchin-like NiCo₂O₄ powders by hydrothermal synthesis for catalytic oxidative desulfurization. *RSC Adv.* **2022**, *12*, 32659–32666. [[CrossRef](#)] [[PubMed](#)]
16. Peng, L.W.; Wang, H.W.; Lv, M.G. A Novel Preparation of Mn/NiCo₂O₄ Catalyst with High Catalytic Activity on Methane. *J. Nanoelectron. Optoelectron.* **2021**, *16*, 926–932. [[CrossRef](#)]
17. Wang, T.; Qiu, L.; Li, H.; Zhang, C.; Sun, Y.; Xi, S.; Ge, J.; Xu, Z.J.; Wang, C. Facile synthesis of palladium incorporated NiCo₂O₄ spinel for low temperature methane combustion: Activate lattice oxygen to promote activity. *J. Catal.* **2021**, *404*, 400–410. [[CrossRef](#)]
18. Zhang, M.; Sui, X.; Zhang, X.; Niu, M.; Li, C.; Wan, H.; Qiao, Z.-A.; Xie, H.; Li, X. Multi-defects engineering of NiCo₂O₄ for catalytic propane oxidation. *Appl. Surf. Sci.* **2022**, *600*, 154040. [[CrossRef](#)]
19. Zhu, Y.; Zuo, Y.; Ye, F.; Zhou, J.; Tang, Y.; Chen, Y. Dual-regulation strategy to enhance electrochemical catalysis ability of NiCo₂O_{4-x} for polysulfides conversion in Li-S batteries. *Chem. Eng. J.* **2022**, *428*, 131109. [[CrossRef](#)]
20. Xing, Y.; Tian, F.; Wu, D.; Yong, X.; Jin, X.; Ni, G. Facile synthesis of Z-scheme ZnMoO₄/Bi₂O₄ heterojunction photocatalyst for effective removal of levofloxacin. *Inorg. Chem. Commun.* **2022**, *143*, 109763. [[CrossRef](#)]
21. Wang, S.; Zhu, J.; Wu, X.; Feng, L. Microwave-assisted hydrothermal synthesis of NiMoO₄ nanorods for high-performance urea electrooxidation. *Chin. Chem. Lett.* **2022**, *33*, 1105–1109. [[CrossRef](#)]
22. Pallavolu, M.R.; Das, H.T.; Kumar, Y.A.; Naushad, M.; Sambasivam, S.; Jung, J.H.; Joo, S.W. Marigold flower-like Sn₃O₄ nanostructures as efficient battery-type electrode material for high-performing asymmetric supercapacitors. *J. Electroanal. Chem.* **2022**, *920*, 116641. [[CrossRef](#)]
23. Simancas, R.; Takemura, M.; Yonezawa, Y.; Sukenaga, S.; Ando, M.; Shibata, H.; Chokkalingam, A.; Iyoki, K.; Okubo, T.; Wakihara, T. Exploring Hydrothermal Synthesis of SAPO-18 under High Hydrostatic Pressure. *Nanomaterials* **2022**, *12*, 396. [[CrossRef](#)]
24. Nguyen, D.T.C.; Vo, D.V.N.; Nguyen, T.T.; Nguyen, T.T.T.; Nguyen, L.T.; Van Tran, T. Optimization of tetracycline adsorption onto zeolitic-imidazolate framework-based carbon using response surface methodology. *Surf. Interfaces* **2022**, *28*, 101549. [[CrossRef](#)]
25. Cao, Y.-F.; Chen, S.-Y.; Zhang, H.-Q.; Feng, J.-H.; Sun, J.-B.; Shi, W.-D. Optimization of magnetization and mechanical properties of Fe-Ni-based alloys by Response Surface Methodology. *Mater. Today Commun.* **2022**, *30*, 103203. [[CrossRef](#)]
26. Boubli, A.; Lebouachera, S.E.; Haddaoui, N.; Guezzout, Z.; Ghriga, M.A.; Hasanzadeh, M.; Drouiche, Y.B.N. State-of-the-art review on recent advances in polymer engineering: Modeling and optimization through response surface methodology approach. *Polym. Bull.* **2022**, *80*, 5999–6031. [[CrossRef](#)]

Disclaimer/Publisher’s Note: The statements, opinions and data contained in all publications are solely those of the individual author(s) and contributor(s) and not of MDPI and/or the editor(s). MDPI and/or the editor(s) disclaim responsibility for any injury to people or property resulting from any ideas, methods, instructions or products referred to in the content.